




# High-performance SERS detection of pesticides using BiOCl-BiOBr@Pt/Au hybrid nanostructures on styrofoams as 3D functional substrate

Ramachandran Balaji<sup>1</sup> · Renganathan Vengudusamy<sup>1</sup> · Shen-Ming Chen<sup>1</sup>  · Tse-Wei Chen<sup>1,2</sup> · Xiaoheng Liu<sup>3</sup> · Mohammad Rizwan Khan<sup>4</sup> · Zeid A. ALOthman<sup>4</sup> · Mohammad Ajmal Ali<sup>5</sup> · Saikh Mohammad Wabaidur<sup>4</sup>

Received: 1 June 2020 / Accepted: 13 September 2020 / Published online: 26 September 2020  
© Springer-Verlag GmbH Austria, part of Springer Nature 2020

## Abstract

A 3D flexible domestic waste styrofoam is reported as a surface enhanced Raman scattering (SERS) substrate loaded with BiOCl-BiOBr@Pt/Au semiconductor-plasmonic composites. The hydrothermally prepared BiOCl-BiOBr nanocomposite is thoroughly characterized for its crystal structure using X-Ray diffraction, morphology through scanning electron microscopy, and electronic states of the elements using X-ray photoelectron spectroscopy. The alpha cypermethrin (ACM) is chosen as a model pesticide analyte for SERS investigation. The BiOCl-BiOBr@Pt/Au loaded foam substrate exhibited a high enhancement factor ( $10^6$ ) and low limit of detection ( $10^{-10}$  M) upon SERS investigation. The unique architecture of the semiconductor-plasmonic composite enables an efficient charge transfer capability and plasmonic hotspots which aids in the enhancement of target analytes. In order to better demonstrate the versatility towards other pesticides, SERS detection of glyphosate and paraquat pesticides are also performed using the fabricated SERS substrate. The stability of the substrate has been investigated in detail for 30 days and the substrate was highly stable. The BiOCl-BiOBr@Pt/Au-based foam substrate also performed well in rapid real-time sensing of alpha cypermethrin on the kiwi fruit exocarp at lower level concentrations.

**Keywords** Semiconductor-plasmonic composites · Styrofoam · SERS · Alpha cypermethrin · Real time sensing

## Introduction

The pesticides are broadly classified into fungicides, herbicides, and insecticides which are diversely consumed in the agricultural sector for eradicating the threat of the pests impairing the cultivational lands and farm animals [1]. Having applied the controlling substance (pesticides) directly

onto the cultivational lands and plants, only a negligible percentage gets transported to the desired target. The inadvertent exposure of the pesticides caused by the solid and liquid waste dumps, spillage, and leaking pipes can conveniently correspond to their dominant existence in the surrounding environment over an extended period of time [2]. As a consequence, this practice of the pesticides has become a pollution and

**Electronic supplementary material** The online version of this article (<https://doi.org/10.1007/s00604-020-04558-3>) contains supplementary material, which is available to authorized users.

✉ Shen-Ming Chen  
smchen78@ms15.hinet.net

✉ Xiaoheng Liu  
xhliu@mail.njust.edu.cn

<sup>1</sup> Department of Chemical Engineering and Biotechnology, National Taipei University of Technology, Taipei 106, Taiwan, Republic of China

<sup>2</sup> Research and Development Center for Smart Textile Technology, National Taipei University of Technology, Taipei 106, Taiwan, Republic of China

<sup>3</sup> Key Laboratory of Education Ministry for Soft Chemistry and Functional Materials, Nanjing University of Science and Technology, Nanjing 210094, China

<sup>4</sup> Department of Chemistry, College of Science, King Saud University, Riyadh 11451, Saudi Arabia

<sup>5</sup> Department of Botany and Microbiology, College of Science, King Saud University, Riyadh 11451, Saudi Arabia

addressing them is one of the prime objectives for the scientific community.

The alpha cypermethrin (ACM) is an emerging class of the synthetic pyrethroid pesticide, and they are heavily consumed in the animal husbandries [3]. The agricultural sector also relies on it due to its low toxicity and good insecticidal action. However, the recent scientific investigation shows the harmful adverse effects of the ACM on the humans [4]. Specifically, the reports suggest that the infants are affected with respiratory issues, nausea, and abnormal changes in the mental condition. In some cases, the overexposure of the ACM has led to brain tumors in the children. Several conventional techniques like electrophoresis and mass spectroscopy are already established for the sensing of ACM but they are not portable and highly time consuming for repetitive examination during the real-time processing [5, 6]. Therefore, we are in need of the portable, fast, point of care, and reliable detection technique for the efficient sensing of ACM like surface enhanced Raman scattering (SERS) [7]. The SERS is progressively becoming one of the precise and selective detection techniques for the pesticides. In the recent years, the SERS has been advanced more with the help of utilization of the nanomaterial embedded surfaces. When the pesticide analyte molecules possessing Raman active bands are adsorbed onto a nanomaterial on the substrates having noble metal-based configuration, a specific enhancement in peaks in the Raman spectrum can be witnessed [8]. The analyte molecule species can be credibly determined by confirming with the molecular fingerprints which has the information on the vibrational bands of the analytes.

The bismuth oxyhalides (BiOCl/BiOBr) are an emerging semiconductor material that have attracted a huge attention owing to their novel crystal structure, less toxic nature, and enhanced catalytic activity than its counterparts [9–12]. The bismuth oxyhalides exhibits a layered tetragonal matlockite structure like Cl-Bi-O-Bi-Cl slabs coherently linked by van der Waals forces. The solid interlayer covalent bonding and frail van der Waals interactions potentially provides a highly enhanced mechanical, electrical, optical, and structural properties [13]. Due to these alluring traits, they are dominantly used for sensing, catalysis, solar cell, nitrogen fixation, hydrogen evolution, and SERS-based applications than other semiconductor based nanocomposites [14–17].

A numerous SERS functional substrate have been fabricated and reported in recent years [18]. The template-based SERS substrates are fabricated using different materials like carbon nanofibers, plasmonic papers, polymers, and graphene [19, 20]. On the flipside, the bioinspired substrates are used as well, for instance, the beetle, dragon fly, and butterfly wings and many leaves and flowers [21–23]. Ideally, these substrates are constructed to support a great amount of the noble metal-based nanocomposites on a 2-dimensional (2D) surface which often results in lower sensitivity. Occurrence of this is due to the laser and Raman scattering having a certain depth of penetration.

Hence, it is better to architect a 3-dimensional (3D) SERS substrate as it increases the volume of sample to laser interaction proving us with a precision fingerprint of the target analyte molecules [24]. The styrofoams are predominantly used in the food and meat packaging sectors. Once the food is consumed, the styrofoam becomes a domesticated waste [25]. In our case, these domesticated waste styrofoam serves as an ideal 3D scaffold matrix for hosting the SERS active semiconductor-plasmonic-based composites. The composites are held intact in the matrix thanks to its superior absorption porosity. There are already reports on the 3D SERS substrates based on Ag sponge, Ni sponge, and Au sponge for the detection of the different analytes [26–28]. This work serves as a first example on the utilization of the 3D styrofoam as a functional substrate for the SERS detection of the harmful pesticides.

In this research work, we have synthesized the BiOCl-BiOBr composite material through a hydrothermal process and subsequently they are thoroughly characterized to understand its crystal structure, morphology, and chemical composition. The domestic waste styrofoam is utilized as an active functional SERS substrate. The BiOCl-BiOBr composite is drop-casted onto the styrofoam and subsequently sputtered coated with Au and Pt (BiOCl-BiOBr@Pt/Au) to make it highly plasmonic which aids in SERS enhancement. The harmful synthetic pesticide alpha cypermethrin (ACM) is used as a pesticide analyte to demonstrate the SERS performance of the fabricated substrate. Our styrofoam substrate displayed an impressive enhancement factor and the limit of detection. The SERS detection of additional pesticides like glyphosate and paraquat is demonstrated to signify that the fabricated SERS substrate is not only applicable to ACM but also for wide ranges of other pesticides. In addition, the substrate is subjected for the reproducibility test and stability test.

## Materials and experimental

### Preparation of 3D styrofoam-based SERS substrates

The 3D domestic waste styrofoam is focused as a working functional substrate for the SERS investigation for ACM detection. The hydrothermally prepared BiOCl-BiOBr [29] (Section S1) is coupled with the thin 10-nm gold (Au) film and 10-nm platinum (Pt) film through a sputter coating on to the styrofoam substrate. The Pt/Au plasmonic heterojunctions on the BiOCl-BiOBr superiorly modifies the surface which improves the SERS activity (BiOCl-BiOBr@Pt/Au). In the SERS investigation, the foam substrate with BiOCl-BiOBr@Pt/Au is used primarily. In an active experiment, a 100  $\mu\text{L}$  of ACM in varying concentrations from  $10^{-5}$  to  $10^{-10}$  M is drop-casted onto the SERS foam substrate. Later, the foam substrate is dried at 50  $^{\circ}\text{C}$  for 2 h. After drying, the foam substrates are utilized for the SERS investigation. The

quality of the foam substrate is investigated through mechanical and thermal characterizations. They are discussed in section S2. All the SERS spectra are collected using a 785-nm laser (10x objective lens) with the exposure time of 10 s and the laser power of 5 mW. The accumulation number for each spectrum is 10 and accumulation cycle time is 3 s. The spot size of each accumulated spectrum is 10  $\mu\text{m}$ . The blank Raman signal is collected at the  $10^{-1}$  M concentration, and the SERS signals are obtained at  $10^{-5}$  M concentration.

## Material characterization

The X-ray diffraction data are collected by using a PerkinElmer PHI-5702 equipped with Cu K $\alpha$  radiation ( $k = 1.54 \text{ \AA}$ ). The surface morphology was observed by field emission scanning electron microscopy (FE-SEM) by Hitachi S-3000 H and the subsequent EDAX is taken using HORIBA EMAX X-ACT (Sensor +24 V = 16 W, resolution at 5.9 keV). The SERS studies are carried out in WITech CRM200 confocal microscopy Raman system with a 785-nm laser. The thermal stability of the styrofoam substrate is tested using thermogravimetric analysis (TGA, METTLER TOLEDO). The stress-strain experiment of the styrofoam substrate is performed using INSTRON 3800R with respect to ASTM638 standard. The TEM images are taken in Shimadzu JEM-1200 EX under an operating voltage of 100 kV. The samples ( $1 \text{ mg mL}^{-1}$  concentration) is drop-casted onto the copper grids and dried at the room temperature prior to the TEM analysis. The material's electronic state and composition is analyzed using XPS. The XPS data is collected from Thermo ESCALAB 11250 instrument equipped with monochromatic Al K $\alpha$  X-ray source (1486.6 eV).

## Choice of materials

Among the various semiconducting composites, the Bi-O-halides-based composites has shown an enhanced catalytic effect upon the incidence of photons. This is due to its highly dispersed valence bands comprising not only O 2p orbitals like metal oxide semiconductors but also Bi 6s orbitals. Bi-O-halide composites have a unique structural organization exhibiting a tetragonal positively charged  $[\text{Bi}_2\text{O}_2]^{2+}$  slabs between the double layers of  $[\text{X}_2]^{2-}$  and halide atoms to form  $[\text{X-Bi-O-Bi-X}]$  layers along the  $c$ -axis. This type of architecture efficiently separates the charge carriers and enables the rapid migration of the charge carriers which benefits the SERS operation. Because of this trait, the BiOCl-BiOBr composites are chosen for the investigation. As an active plasmonic region, the heterojunctions of Pt/Au are preferred. The sputtered plasmonic heterojunctions are wrapped around the BiOCl-BiOBr composites which forms a plasmonic hotspots for further enhancement of the SERS signals.

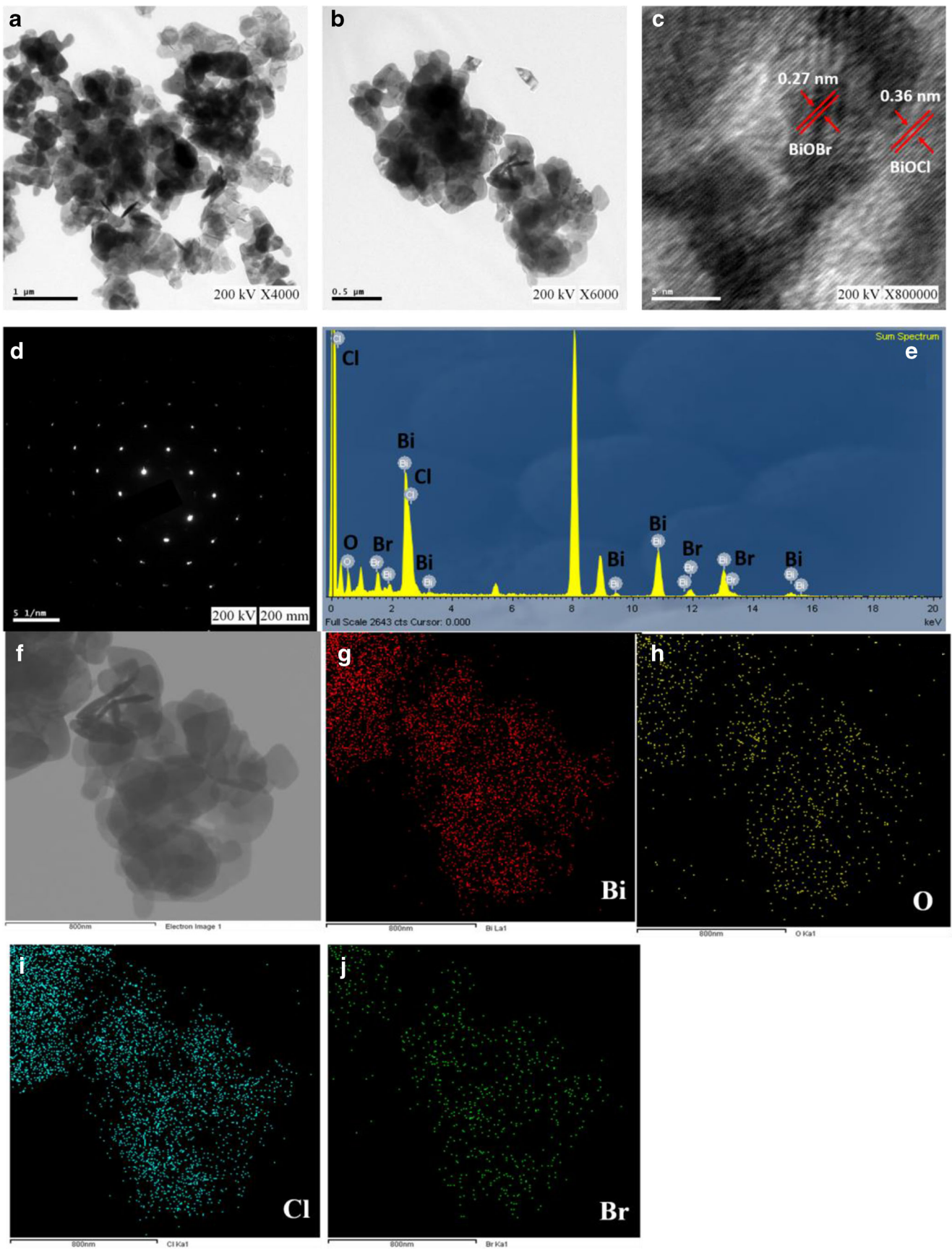
## Results and discussion

### Physical characterization of BiOCl-BiOBr nanocomposites

The purity and the crystal phase of the hydrothermally prepared material is investigated using the powder XRD study. It can be seen in Fig. S2 and discussed in section S3. The surface morphology of the synthesized material is characterized using a scanning electron microscopy. Figure S3a and b shows the SEM images of BiOCl-BiOBr composites. It is clearly seen from the images that multiple BiOCl slabs fuse together to give a flower-like morphology and BiOBr having a pellet like structure is scattered around the BiOCl. The intimate contact between the BiOCl and BiOBr promotes an efficient charge transport which holds a greater importance in the catalysis. The average diameter of the BiOCl flower-like structures is approximately 1  $\mu\text{m}$  and the average diameter of the BiOBr pellet-like material is around 0.2  $\mu\text{m}$ . Upon closer look at the BiOCl-BiOBr composites (Fig. S3b), the fusing of numerous slabs of BiOCl is visible and the thickness of the slabs is around 5–10 nm. The EDAX is carried out for the BiOCl-BiOBr composites and it is shown in Fig. S3c. The elemental mapping for the BiOCl-BiOBr composite is shown in Fig. S4. The presence of all the individual elements in the composite is thereby confirmed.

Figure 1a and b show the TEM images of BiOCl-BiOBr composites where it is clearly evident that the composites are arranged in a cluster of nanosheet-like topography. Figure 1c is the HR-TEM image of the BiOCl-BiOBr composite. We identified the presence of two set of lattice fringes with the inter fringe spacing of 0.36 nm and 0.27 nm which respectively belongs to BiOCl (110) and BiOBr (001). Figure 1d represents the SAED pattern of the composites, in which the dominant distribution of (001) lattice of BiOBr is visible. This pattern is apparent due to the wrapping of the BiOBr over the BiOCl nanoparticles. Figure 1e is the obtained by the EDAX spectrum from the TEM analysis. The presence of Bi, O, Cl, and Br elements are evident proving the formation of the BiOCl-BiOBr composites. Further, the elemental mapping of the BiOCl-BiOBr composites are done and presented in Fig. 1f–j. Figure 1f is the area of survey for the elemental mapping. Figure 1g–j is the mapping of an individual element distributed on the composite in the order of Bi (red), O (yellow), chlorine (blue), and bromine (Br). The elemental mapping firmly confirms the existence of all the elements in the BiOCl-BiOBr composites.

In order to investigate the chemical composition and the electronic state of the elements present in the BiOCl-BiOBr composites, the XPS analysis is performed. The corresponding XPS spectra are presented in Fig. 2. Figure 2a shows the complete survey spectrum of the composite material. From Fig. 2b, the two peaks arising at binding energy of 160 eV



◀ **Fig. 1** TEM images of (a, b) BiOCl-BiOBr. (c) HR-TEM image of BiOCl-BiOBr. (d) SAED pattern of BiOCl-BiOBr. (e) EDAX spectrum of BiOCl-BiOBr. (f) Chosen region for elemental mapping analysis, (g) Bi distribution, (h) O distribution, (i) Cl distribution, and (j) Br distribution

and 167 eV are for the Bi 4f<sub>7/2</sub> and Bi 4f<sub>5/2</sub>. This confirms the presence of the Bi<sup>3+</sup> ions in the BiOCl-BiOBr composites. The peak at binding energy 535 eV is assigned to O 1s (Fig. 2c). Figure 2d exhibits a binding energy peak at 201 eV which is for the Cl 2p state and characteristic to the presence of Cl<sup>-</sup> ions in the composite. The presence of Br<sup>-</sup> anions can be seen at the binding energy peak originating at 71 eV in Br 3d electronic state (Fig. 2e). Therefore, the XRD and the XPS analyzed data serves as an evidence for coexistence of BiOCl and BiOBr is accomplished in the desired BiOCl-BiOBr composites.

### SERS enhancement factor (EF) investigation of the 3D styrofoam substrates

Scheme S1 presents the diagrammatic representation of the fabrication of styrofoam-based SERS active substrates. The FS 1 is the bare styrofoam substrate, the FS 2 is the BiOCl-BiOBr composite on the styrofoam substrate, the FS 3 is the

BiOCl-BiOBr/Pt combination on the styrofoam substrate, the FS 4 is the BiOCl-BiOBr/Au combination on the substrate, and finally, FS 5 is the BiOCl-BiOBr@Pt/Au semiconductor-plasmonic composite combination on the styrofoam substrate which is the primary substrate for the investigation.

The SERS performance of primary substrate FS 5 and control substrates FS (1–4) is investigated by utilizing ACM as a model analyte. In order to understand the morphology of styrofoam before and after hosting the BiOCl-BiOBr@Pt/Au composites, the SEM characterizations are done. Figure 3a and b show the SEM image of the bare styrofoam before BiOCl-BiOBr@Pt/Au composite loading and Fig. 3c and d show the SEM image of styrofoam after the BiOCl-BiOBr@Pt/Au composite loading. It is clearly evident from the images that the intended composites are successfully aligned as an aggregate on each network of the styrofoam (FS 5) and making them SERS active. These semiconductor-plasmonic composite actively plays an important role in the charge transfer process and the formation of plasmonic hotspots which helps in the SERS process. Furthermore, scanning electron microscope (SEM) mapping of elements and EDAX is carried out for the main FS 5 substrate (Fig. 3e–l) which undoubtedly confirms the presence of bismuth (Bi), oxygen (O), chlorine (Cl), bromine (Br), platinum (Pt), and gold (Au) on the styrofoam substrate. The real-time fabrication of the FS substrates is depicted in the Scheme S2. Figure 4

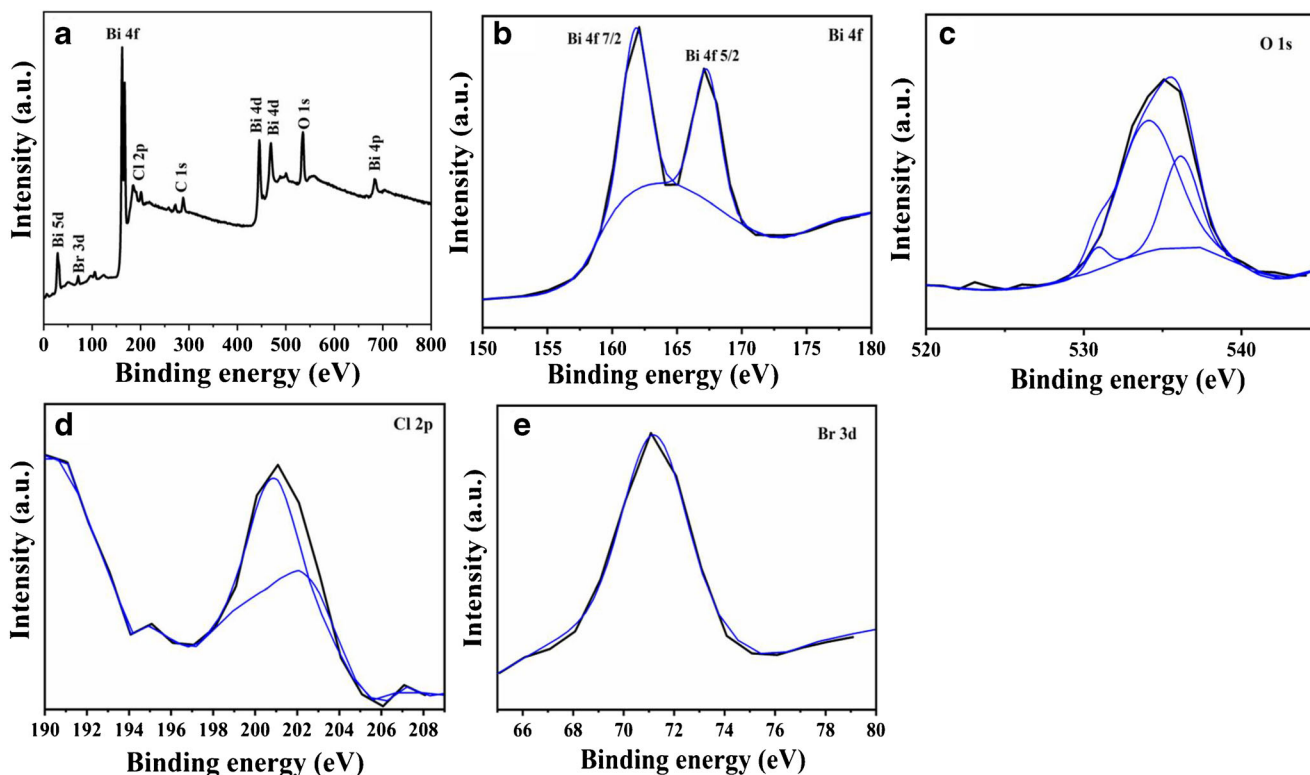


**Fig. 2** XPS investigation of BiOCl-BiOBr composites in the (a) survey spectrum, (b) Bi 4f spectrum, (c) O 1s spectrum, (d) Cl 2p spectrum, and (e) Br 2d spectrum

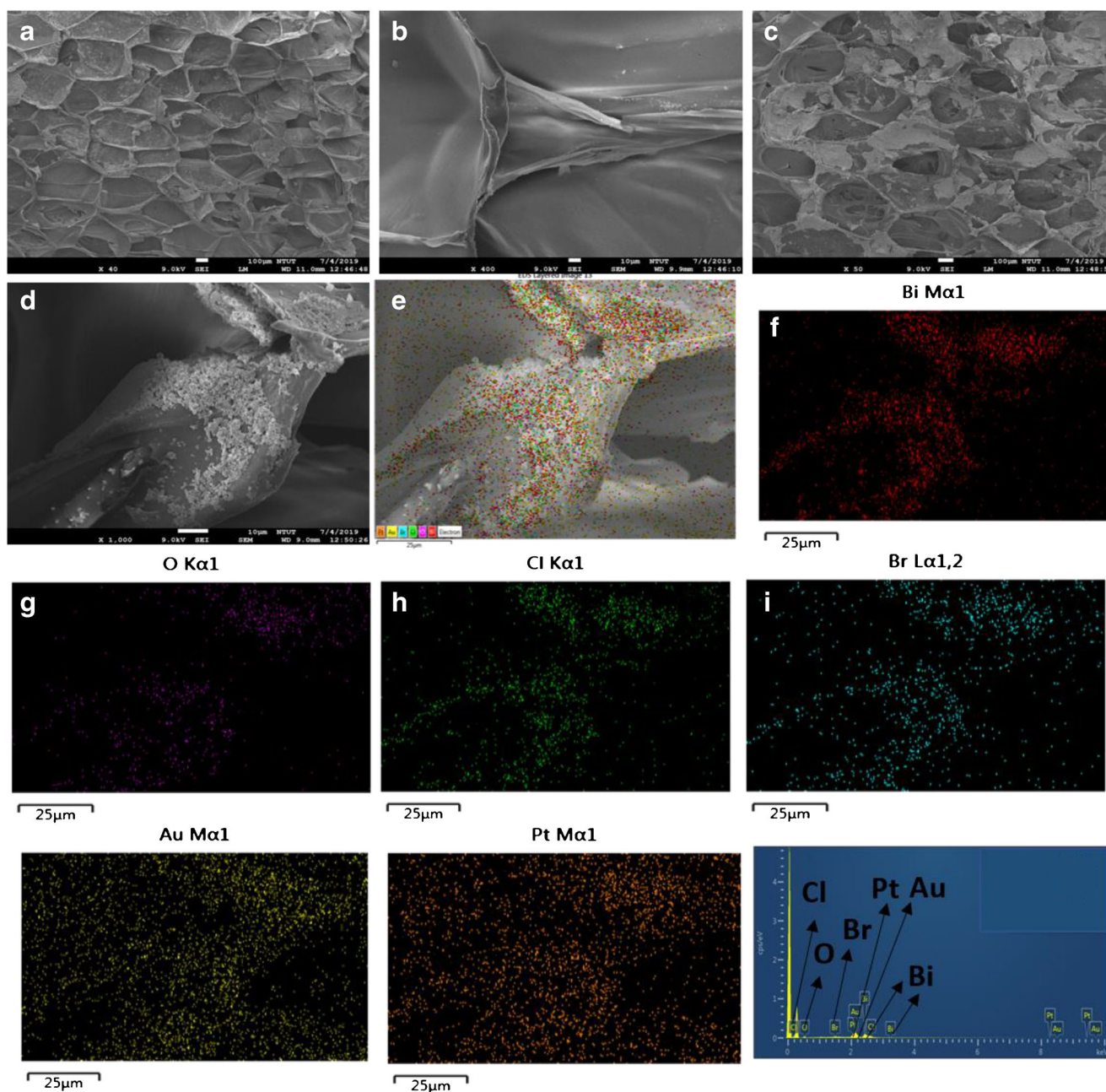


**Fig. 3** SEM images of (a, b) bare styrofoam and (c, d) BiOCl-BiOBr@Pt/Au on styrofoam. Elemental mapping of FS 5 substrate (e) surveyed area, (f) Bi, (g) O, (h) Cl, (i) Br, (j) Au, (k) Pt, and (l) EDAX spectrum of the mapped region

shows the SERS spectra of ACM molecules on various fabricated 3D foam substrates (FS 1, FS 2, FS 3, FS 4, and FS 5), and its corresponding characteristic peaks are indexed. The intermediates observed during the detection of ACM are 3-phenoxybenzoic acid ( $1011\text{ cm}^{-1}$ ,  $1190\text{ cm}^{-1}$ , and  $3070\text{ cm}^{-1}$ ) and cyclopropane carboxylic acid ( $1320\text{ cm}^{-1}$ ,  $1617\text{ cm}^{-1}$ ). The evaluation of enhancement factor (EF) of ACM on foam is estimated with the mentioned equation and the data is listed in Table S1.

$$EF = \frac{I_{\text{SERS}}/C_{\text{SERS}}}{I_{\text{RS}}/C_{\text{RS}}}$$

In which, the  $I_{\text{SERS}}$  represents enhancement in the intensity of signal,  $C_{\text{SERS}}$  is the analyte concentration (ACM) in SERS spectra,  $I_{\text{RS}}$  is signal of blank Raman spectra of ACM, and  $C_{\text{RS}}$  indicates the ACM concentration without the SERS functional substrate. In all of the cases with respect to foam substrates (FS

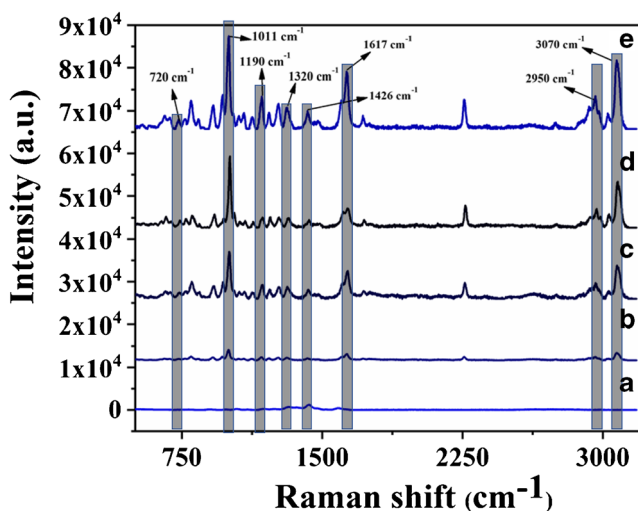


**Fig. 4** ACM SERS spectra for  $10^{-5}$  M concentration (a) FS 1, (b) FS 2, (c) FS 3, (d) FS 4, and (e) FS 5 substrates. SERS spectra are collected using a 785-nm laser (10x objective lens) with the exposure time of 10 s and the laser power of 5 mW. The accumulation number for each spectrum is 10 and accumulation cycle time is 3 s. The spot size of each accumulated spectrum is  $10\ \mu\text{m}$

1, FS 2, FS 3, FS 4, and FS 5), we equated the obtained the SERS spectrum in comparison with the blank ACM (FS 1 at  $10^{-1}$  M). From the measurements, it is confirmed that BiOCl-BiOBr@Pt/Au @ styrofoam SERS substrate (FS 5) consisting a semiconductor-plasmonic configuration disclosed a high EF when compared with others (FS 1, FS 2, FS 3, and FS 4). This is mainly because of the energy transfer occurring between the BiOCl-BiOBr and Pt/Au nanothin film surface. This energy process helps to increase the electromagnetic hotspots and respectively in the enhancement of pesticide analyte (ACM) molecules signal intensity. The influence of the BiOCl-BiOBr composites is discussed in section S4. Therefore, SERS study

demonstrates that 3D BiOCl-BiOBr@Pt/Au@styrofoam SERS substrates are highly recommended for real-time SERS detection of toxic pesticides.

### Limit of detection (LOD) investigation of the SERS styrofoam substrate

The investigation for the limit of detection (LOD) of the FS 5 substrate is carried out and the obtained data is depicted in Fig. 5a. In a typical LOD experiment, on the FS5, the ACM in the different concentrations are taken, drop-casted ( $100\ \mu\text{L}$ ), and further dried prior to the experiment. After the LOD investigation, the FS 5 displayed a hugely sensitive SERS sensing capability with the LOD of  $10^{-10}$  M. The estimation of LOD is briefed in section S5. This ultrasensitive detection of ACM is due to the unique semiconductor/plasmonic architecture. Figure 5b shows a linear relationship between the concentration of the ACM and SERS intensity of the analyte molecules. Table 1 shows the performance comparison of various SERS substrates and materials that are very recently reported to that of our fabricated styrofoam-based SERS substrate showing the analytical figures of merits like LOD and EF.

### Reproducibility, selectivity, and stability investigation of the SERS styrofoam substrate

The FS 5 substrate is also subjected for the signal reproducibility study at the lower level concentration ( $10^{-10}$  M). The results are displayed in Fig. S6. In this study, the SERS experiments are done using the FS 5 substrates containing  $10^{-10}$  M concentration of ACM molecules. Then, in 10 randomly selected areas, SERS investigation is done and its respective data is displayed in Fig. S6a. From Fig. S6b, it is confirmed that the SERS signals almost have a similar intensity which goes on to suggest that the FS 5 surface provides a

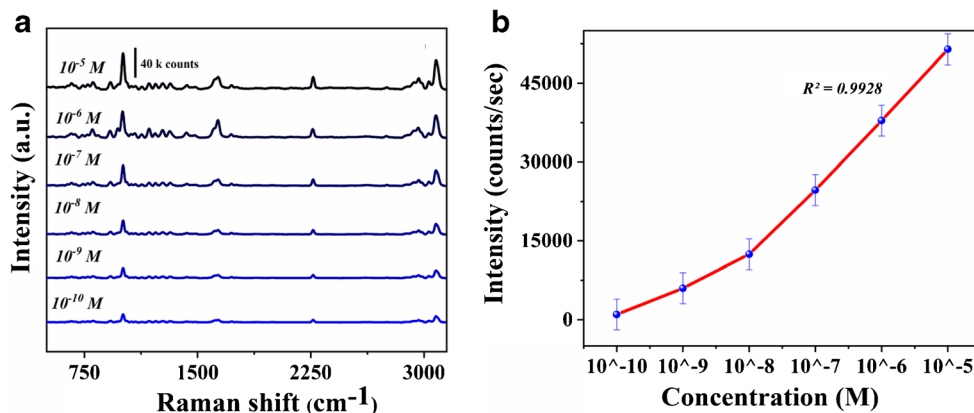


**Fig. 5** (a) Concentration-dependent studies using primary FS 5 substrate and (b) linear plot for the concentration against the SERS intensity for the peak  $1011\ \text{cm}^{-1}$ . The error bars indicate the standard deviation from at least 10 spectra. SERS spectra are collected using a 785-nm laser (10x

objective lens) with the exposure time of 10 s and the laser power of 5 mW. The accumulation number for each spectrum is 10 and accumulation cycle time is 3 s. The spot size of each accumulated spectrum is  $10\ \mu\text{m}$

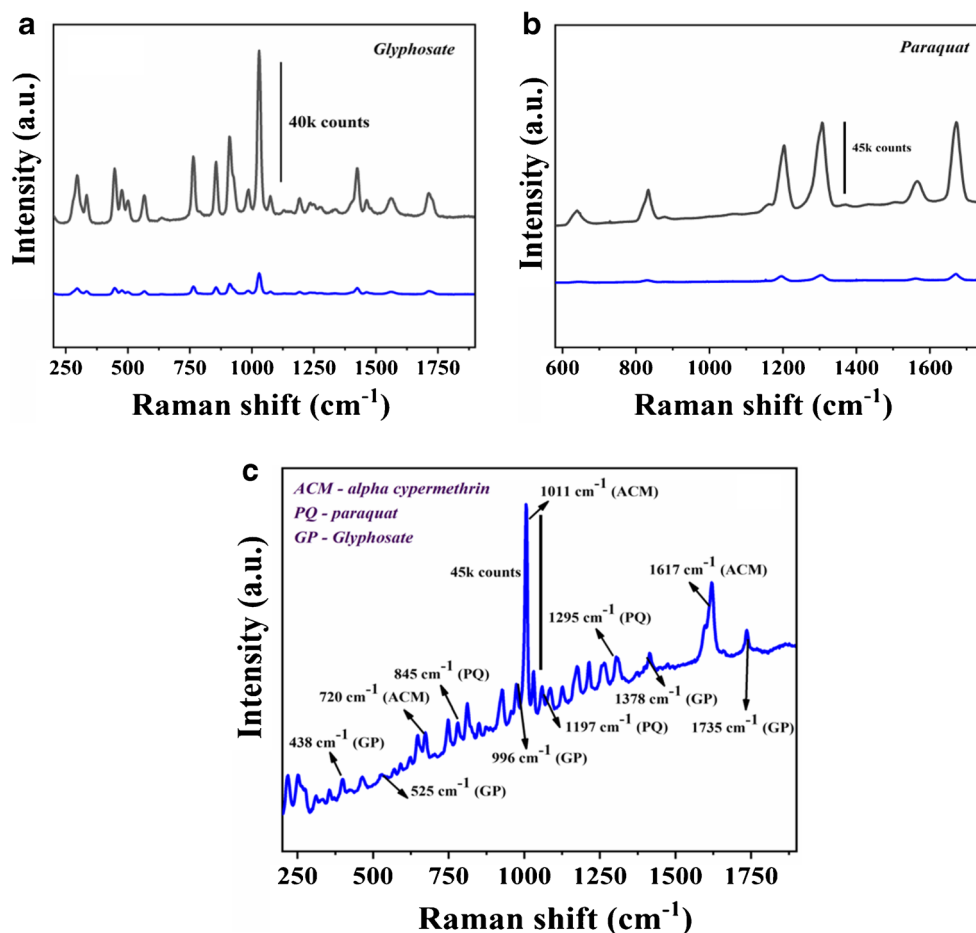
**Table 1** Comparison table of SERS detection of various pesticides showing the type of material used, substrates used, choice of pesticide, limit of detection, and the enhancement factor

Material utilized	Substrate used	Choice of pesticide	Limit of detection (M)	Enhancement factor	References
Flower-like MoS <sub>2</sub> @Ag hybrid	Material itself	Methyl parathion	10 <sup>-7</sup>	10 <sup>8</sup>	[30]
ZnO/Ag nanocomposites	Filter paper	Dimethoate	10 <sup>-5</sup>	10 <sup>4</sup>	[31]
Au@ Ag-cysteamine	Material itself	Oxamyl	10 <sup>-7</sup>	–	[32]
Ag colloids	Material itself	Thiabendazole	10 <sup>-8</sup>	10 <sup>6</sup>	[33]
Hexagonal-BN/CuAg nanoalloys	Tomato skin	Tricyclazole	10 <sup>-7</sup>	–	[34]
Balsam pear-shaped CuO nanostructures	Material itself	Paraquat	10 <sup>-6</sup>	–	[35]
AgFeO <sub>2</sub> @Au/Ag nanoparticles	Material itself	Paraoxon ethyl	10 <sup>-8</sup>	10 <sup>6</sup>	[36]
BiOCl-BiOBr@Pt/Au	Domestic waste styrofoam	Alpha cypermethrin	10 <sup>-10</sup>	10 <sup>6</sup>	This Research work

uniform SERS signals. The relative standard deviation (RSD) is evaluated as 7.42% for the ACM with the concentration of 10<sup>-10</sup> M. Figure S7 shows the SEM image of the primary FS 5 substrate after the reproducibility studies, in which the substrate had the BiOCl-BiOBr@Pt/Au composite material intact showing the efficient hosting capability of the 3D styrofoams.

In order to exhibit the versatility of the BiOCl-BiOBr@Pt/Au-based foam substrate, we have also additionally investigated with other hazardous pesticides like glyphosate (GP) and paraquat (PQ). Figure 6a shows the SERS spectra of the GP (gray) which presented a significant enhancement from the blank spectra (blue), and similarly, Fig. 6b shows the enhanced characteristic peaks PQ in the

**Fig. 6** (a) SERS analysis of glyphosate (GP). (b) SERS analysis of paraquat (PQ). (c) SERS analysis of mixed pesticides (ACM, PQ, and GP). SERS spectra are collected using a 785-nm laser (10x objective lens) with the exposure time of 10 s and the laser power of 5 mW. The accumulation number for each spectrum is 10 and accumulation cycle time is 3 s. The spot size of each accumulated spectrum is 10 μm





SERS spectra (blue). These SERS experiments are performed under the identical conditions of the ACM measurements. Additionally, all the three pesticides (ACM, PQ, and GP) are mixed together in the  $10^{-5}$  M concentration and SERS measurement is done on the FS 5 substrate. Figure 6c shows the enhanced characteristic peaks of all the pesticides utilized. This clearly proves that our fabricated BiOCl-BiOBr@Pt/Au-based foam substrate is not only limited to ACM but also can be used for wide spectra of other harmful pesticides. Figure S8a reports the stability of the FS 5 substrate for the period of 30 days. All the SERS data is collected at the  $10^{-5}$  M concentration of ACM. The decrement in the SERS intensity of the ACM is noted at the 30th day but they were negligible and all the characteristic peaks of the ACM is evident. This shows the impressive stability of the FS 5 substrate. At the end of stability study, the SEM images of the FS 5 substrate is taken and it is displayed in Fig. S8b. We can clearly see that the morphology of the BiOCl-BiOBr composite is unperturbed and intact proving the stability of the composites.

### SERS enhancement mechanism on the styrofoam substrates

The mechanism that rules the SERS activity on the 3D styrofoam substrate is shown in Scheme S3. The architecture of semiconductor/plasmonic heterojunction combination

(BiOCl-BiOBr@Pt/Au) are in close contact with each other. Because of this architecture, an efficient charge transfer is occurring from BiOCl-BiOBr to the plasmonic Pt/Au nanothin film which has a localized surface plasmon resonance. Therefore, the FS 5 combination of the styrofoam substrate is highly sensitive towards the detection of ACM molecules. Furthermore, the enhancement of the electromagnetic field in multiple orders happens in the Pt/Au nanothin film which leads to the formation of numerous surface plasmonic regions. Due to these, enhancement of the SERS signal of ACM occurs in these Pt/Au regions. The assembly of Pt/Au nanofilm on to the surface of BiOCl-BiOBr forms a nanocomposite. The nanocomposite induces the numerous electromagnetic hotspot and SERS signal enhancement. Also, the mechanism of charge transfer also enjoys a vital role in SERS enhancement. The molecule's polarizability caused by the laser excitation is explained as  $\alpha_{\sigma p} = S + A$ , where the  $S$  and  $A$  represent the photon-induced transfer of charges from the analyte molecules to the surface of nanomaterial and vice versa. The photon-induced transfer of charges in surface enhanced Raman scattering can be broken down. Initially, the charge transfer occurs from BiOCl-BiOBr to the analyte, i.e., the incident photons from the laser excitation and the charges from BiOCl-BiOBr are excited to mid energy levels and later transfer to LUMO of the analyte. Finally, the charge transfer happens from ground state of completely occupied analyte molecule to the BiOCl.

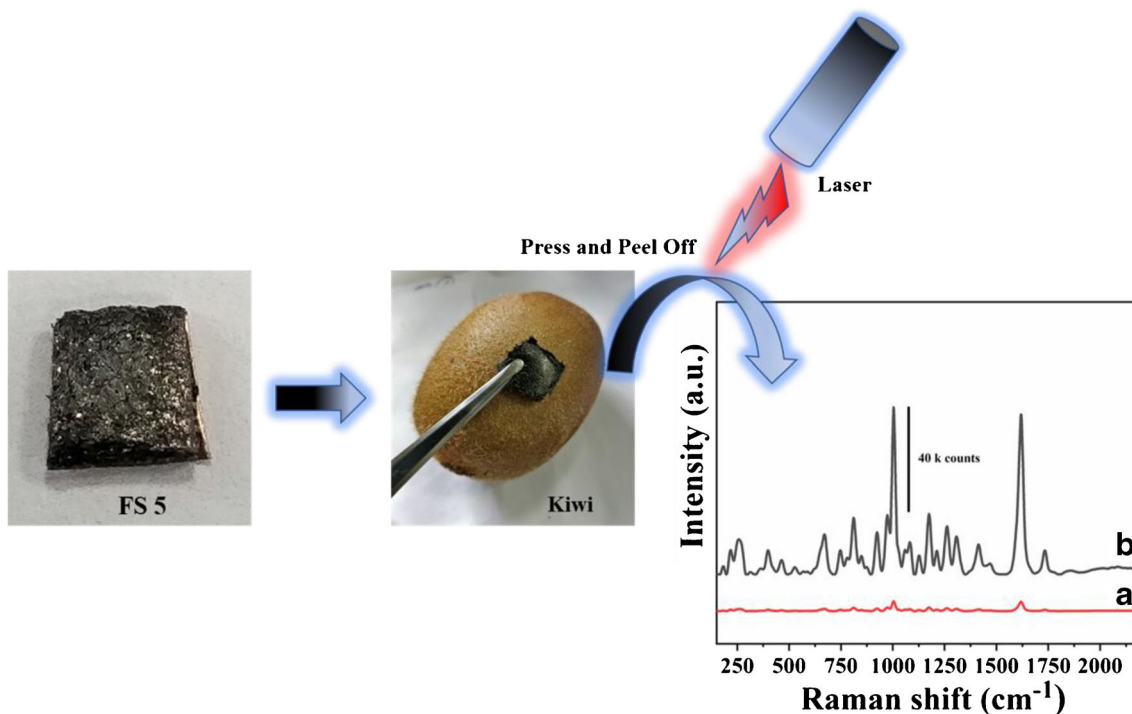


**Fig. 7** Process of real sample analysis and the SERS data obtained. (a) Blank Raman signal at a  $10^{-1}$  M concentration and (b) SERS signal at  $10^{-5}$  M concentration. SERS spectrum is collected using a 785 nm laser (10x objective lens) with the exposure time of 10 s and the laser power of

5 mW. The accumulation number for each spectrum is 10 and accumulation cycle time is 3 s. The spot size of each accumulated spectrum is 10  $\mu$ m

## Application to the analysis of real samples using SERS styrofoam substrate

In the practical consumer production, pesticides are often sprayed on the fruits and vegetables which results in the multiple folds of pesticide residues. These residues put the human life in danger of numerous health hazards. Based on the investigated 3D styrofoam SERS substrate BiOCl-BiOBr@Pt/Au (FS 5), these pesticides can be precisely fingerprinted in real time. In order to demonstrate the practical application of the FS 5, the ACM is determined on the kiwi fruit exocarp. The ACM pesticide molecules is sprayed ( $10^{-5}$  M concentration) on the exocarp of the kiwi fruit and the respective SERS investigated data is presented in the Fig. 7. The SERS signal exhibited all the characteristic peaks for the ACM ( $1011\text{ cm}^{-1}$ ,  $1190\text{ cm}^{-1}$ ,  $1320\text{ cm}^{-1}$ ,  $1617\text{ cm}^{-1}$ , and  $1426\text{ cm}^{-1}$ ) with a remarkable EF of  $10^6$  intended for the  $1011\text{ cm}^{-1}$  peak which shows the efficient sensing capacity of the styrofoam-based substrate (FS 5). Before the real-time investigation, the glass slides containing the BiOCl-BiOBr@Pt/Au composites are used as a reference material and the corresponding data is shown in Fig. S9. Upon investigation using reference material, we obtained an enhancement factor up to  $10^3$  which is far inferior to our FS 5 substrate. This indicates the enhanced SERS capability of the primary FS 5 substrate. Therefore, our SERS substrate can be used for the rapid detection of various pesticides on the fruits in the real-world conditions.

## Conclusion

We present a rapid, effective, and portable BiOCl-BiOBr@Pt/Au composite-based SERS platform for the fingerprinting of the pesticide alpha cypermethrin. The domestic food container waste styrofoam is used as a substrate for hosting the composites for SERS detection. Upon the SERS investigation, we obtained highly promising results with the multifold enhancement in the SERS signal of the analyte and impressive limit of detection. The real-time detection of pesticides on the exocarp of kiwi fruit is successfully demonstrated. In the future, we also aim to develop a SERS substrate which can efficiently operate in the elevated temperature as our current styrofoam substrate degrades at  $380\text{ }^\circ\text{C}$ . The developed SERS substrate based on BiOCl-BiOBr@Pt/Au composites in this work not only exhibits the potential for detection of alpha cypermethrin pesticide but also can be employed for the other wide range of pesticides. Therefore, the styrofoam-based SERS substrate can be used in the real-world consumer market for the rapid monitoring of various pesticides exposed on fruits.

**Funding** This work is jointly supported by the projects from NTUT-NUST-109-01 and NSFC51872141, National Taipei University of Technology and Nanjing University of Science and Technology. This project is supported by the Ministry of Science and Technology (MOST 107-2113-M-027-005-MY3), Taiwan. This work is funded by the Researchers Supporting Project Number (RSP-2020/138) King Saud University, Riyadh, Saudi Arabia.

## Compliance with ethical standards

**Conflict of interest** There are no conflicts of interest to declare.

## References

- Eddleston M, Karalliedde L, Buckley N, Fernando R, Hutchinson G, Isbister G, Konradsen F, Murray D, Piola JC, Senanayake N, Sheriff R, Singh S, Siwach SB, Smit L (2002) Pesticide poisoning in the developing world—a minimum pesticides list. *Lancet* 360(9340):1163–1167. [https://doi.org/10.1016/S0140-6736\(02\)11204-9](https://doi.org/10.1016/S0140-6736(02)11204-9)
- Pereira JL, Antunes SC, Castro BB, Marques CR, Gonçalves AM, Gonçalves F, Pereira R (2009) Toxicity evaluation of three pesticides on non-target aquatic and soil organisms: commercial formulation versus active ingredient. *Ecotoxicology* 18(4):455–463. <https://doi.org/10.1007/s10646-009-0300-y>
- Amweg EL, Weston DP, Ureda NM (2005) Use and toxicity of pyrethroid pesticides in the Central Valley, California, USA. *Environ Toxicol Chem* 24(4):966–972. <https://doi.org/10.1897/04-146R1.1>
- Saillenfait A-M, Ndiaye D, Sabaté J-P (2015) Pyrethroids: exposure and health effects—an update. *Int J Hyg Environ Health* 218(3):281–292. <https://doi.org/10.1016/j.ijheh.2015.01.002>
- Ramesh A, Ravi PE (2004) Electron ionization gas chromatography–mass spectrometric determination of residues of thirteen pyrethroid insecticides in whole blood. *J Chromatogr B* 802(2):371–376. <https://doi.org/10.1016/j.jchromb.2003.12.016>
- Li X, Yang T, Song Y, Zhu J, Wang D, Li W (2019) Surface-enhanced Raman spectroscopy (SERS)-based immunochromatographic assay (ICA) for the simultaneous detection of two pyrethroid pesticides. *Sensors Actuators B Chem* 283:230–238. <https://doi.org/10.1016/j.snb.2018.11.112>
- Pang S, Yang T, He L (2016) Review of surface enhanced Raman spectroscopic (SERS) detection of synthetic chemical pesticides. *Trends Anal Chem* 85:73–82. <https://doi.org/10.1016/j.trac.2016.06.017>
- Alvarez-Puebla RA, Liz-Marzán LM (2012) SERS detection of small inorganic molecules and ions. *Angew Chem Int Ed* 51(45):11214–11223. <https://doi.org/10.1002/anie.201204438>
- Khan SB, Alamry KA, Marwani HM, Asiri AM, Rahman MM (2013) Synthesis and environmental applications of cellulose/ZrO<sub>2</sub> nanohybrid as a selective adsorbent for nickel ion. *Compos B Eng* 50:253–258. <https://doi.org/10.1016/j.compositesb.2013.02.009>
- Rahman MM, Khan SB, Asiri AM, Marwani HM, Qusti AH (2013) Selective detection of toxic Pb (II) ions based on wet-chemically prepared nanosheets integrated CuO–ZnO nanocomposites. *Compos B Eng* 54:215–223. <https://doi.org/10.1016/j.compositesb.2013.05.018>
- Khan A, Asiri AM, Khan AAP, Rub MA, Azum N, Rahman MM, Al-Youbi AO, Qusti AH (2014) Dual nature, self oxidized poly (o-anisidine) functionalized multiwall carbon nanotubes composite: preparation, thermal and electrical studies. *Compos B Eng* 58:451–456. <https://doi.org/10.1016/j.compositesb.2013.10.059>

12. Ahmed J, Rahman MM, Siddiquey IA, Asiri AM, Hasnat MA (2018) Efficient hydroquinone sensor based on zinc, strontium and nickel based ternary metal oxide (TMO) composites by differential pulse voltammetry. *Sensors Actuators B Chem* 256:383–392. <https://doi.org/10.1016/j.snb.2017.10.076>
13. Balaji R, Renganathan V, Chen S-M, Singh V (2020) Ingenious design and development of recyclable 2D BiOCl nanotiles attached tri-functional robust strips for high performance selective electrochemical sensing, SERS and heterogenous dip catalysis. *Chem Eng J* 385:123974. <https://doi.org/10.1016/j.cej.2019.123974>
14. Awual MR, Hasan MM, Asiri AM, Rahman MM (2019) Cleaning the arsenic (V) contaminated water for safe-guarding the public health using novel composite material. *Compos B Eng* 171:294–301. <https://doi.org/10.1016/j.compositesb.2019.05.078>
15. Karim MR, Alam M, Ajjaz M, Asiri AM, Dar M, Rahman MM (2019) Fabrication of 1, 4-dioxane sensor based on microwave assisted PAni-SiO<sub>2</sub> nanocomposites. *Talanta* 193:64–69. <https://doi.org/10.1016/j.talanta.2018.09.100>
16. Katowah DF, Rahman MM, Hussein MA, Sobahi T, Gabal M, Alam M, Asiri AM (2019) Ternary nanocomposite based poly (pyrrole-co-O-toluidine), cobalt ferrite and decorated chitosan as a selective Co<sup>2+</sup> cationic sensor. *Compos B Eng* 175:107175. <https://doi.org/10.1016/j.compositesb.2019.107175>
17. Ahmed J, Rahman MM, Siddiquey IA, Asiri AM, Hasnat MA (2017) Efficient Bisphenol-A detection based on the ternary metal oxide (TMO) composite by electrochemical approaches. *Electrochim Acta* 246:597–605. <https://doi.org/10.1016/j.electacta.2017.06.072>
18. Zhang Y, Liu S, Wang L, Qin X, Tian J, Lu W, Chang G, Sun X (2012) One-pot green synthesis of Ag nanoparticles-graphene nanocomposites and their applications in SERS, H<sub>2</sub>O<sub>2</sub>, and glucose sensing. *RSC Adv* 2(2):538–545. <https://doi.org/10.1039/c1ra00641j>
19. Alam MK, Rahman MM, Elzawy A, Torati SR, Islam MS, Todo M, Asiri AM, Kim D, Kim C (2017) Highly sensitive and selective detection of Bis-phenol A based on hydroxyapatite decorated reduced graphene oxide nanocomposites. *Electrochim Acta* 241:353–361. <https://doi.org/10.1016/j.electacta.2017.04.135>
20. Wang L, Li H, Tian J, Sun X (2010) Monodisperse, micrometer-scale, highly crystalline, nanotextured Ag dendrites: rapid, large-scale, wet-chemical synthesis and their application as SERS substrates. *ACS Appl Mater Interfaces* 2(11):2987–2991. <https://doi.org/10.1021/am100968j>
21. Wang Y, Wang M, Shen L, Sun X, Shi G, Ma W, Yan X (2018) High-performance flexible surface-enhanced Raman scattering substrates fabricated by depositing Ag nanoislands on the dragonfly wing. *Appl Surf Sci* 436:391–397. <https://doi.org/10.1016/j.apsusc.2017.11.212>
22. Garrett NL, Sekine R, Dixon MW, Tilley L, Bamberg KR, Wood BR (2015) Bio-sensing with butterfly wings: naturally occurring nano-structures for SERS-based malaria parasite detection. *Phys Chem Chem Phys* 17(33):21164–21168. <https://doi.org/10.1039/C4CP04930F>
23. Chou S-Y, Yu C-C, Yen Y-T, Lin K-T, Chen H-L, Su W-F (2015) Romantic story or Raman scattering? Rose petals as ecofriendly, low-cost substrates for ultrasensitive surface-enhanced Raman scattering. *Anal Chem* 87(12):6017–6024. <https://doi.org/10.1021/acs.analchem.5b00551>
24. Srichan C, Ekpanyapong M, Horprathum M, Eiamchai P, Nuntawong N, Phokharatkul D, Danvirutai P, Bohez E, Wisitsoraat A, Tuantranont A (2016) Highly-sensitive surface-enhanced Raman spectroscopy (SERS)-based chemical sensor using 3D graphene foam decorated with silver nanoparticles as SERS substrate. *Sci Rep* 6:23733. <https://doi.org/10.1038/srep23733>
25. Hawkins G (2018) The skin of commerce: governing through plastic food packaging. *J Cult Econ* 11(5):386–403. <https://doi.org/10.1080/17530350.2018.1463864>
26. Khan A, Asiri AM, Rub MA, Azum N, Khan AAP, Khan SB, Rahman MM, Khan I (2013) Synthesis, characterization of silver nanoparticle embedded polyaniline tungstophosphate-nanocomposite cation exchanger and its application for heavy metal selective membrane. *Compos B Eng* 45(1):1486–1492. <https://doi.org/10.1016/j.compositesb.2012.09.023>
27. Zhang T, Zhou F, Hang L, Sun Y, Liu D, Li H, Liu G, Lyu X, Li C, Cai W, Li Y (2017) Controlled synthesis of sponge-like porous Au–Ag alloy nanocubes for surface-enhanced Raman scattering properties. *J Mater Chem C* 5(42):11039–11045. <https://doi.org/10.1039/C7TC03855K>
28. Sun J, Gong L, Lu Y, Wang D, Gong Z, Fan M (2018) Dual functional PDMS sponge SERS substrate for the on-site detection of pesticides both on fruit surfaces and in juice. *Analyst* 143(11):2689–2695. <https://doi.org/10.1039/C8AN00476E>
29. Zhang X, Ai Z, Jia F, Zhang L (2008) Generalized one-pot synthesis, characterization, and photocatalytic activity of hierarchical BiOX (X= Cl, Br, I) nanoplate microspheres. *J Phys Chem C* 112(3):747–753. <https://doi.org/10.1021/jp077471t>
30. Chen Y, Liu H, Tian Y, Du Y, Ma Y, Zeng S, Gu C, Jiang T, Zhou J (2020) In situ recyclable surface-enhanced Raman scattering-based detection of multicomponent pesticide residues on fruits and vegetables by the flower-like MoS<sub>2</sub>@ Ag hybrid substrate. *ACS Appl Mater Interfaces* 12(12):14386–14399. <https://doi.org/10.1021/acsami.9b22725>
31. Jin X, Guo P, Guan P, Wang S, Lei Y, Wang G (2020) The fabrication of paper separation channel based SERS substrate and its recyclable separation and detection of pesticides. *Spectrochim Acta A* 118561. <https://doi.org/10.1016/j.saa.2020.118561>
32. Hussain A, Pu H, Sun D-W (2020) Cysteamine modified core-shell nanoparticles for rapid assessment of oxamyl and thiacloprid pesticides in milk using SERS. *J Food Meas Charact* 14:2021–2029. <https://doi.org/10.1007/s11694-020-00448-7>
33. Oliveira MJ, Rubira RJ, Furini LN, Batagin-Neto A, Constantino C (2020) Detection of thiabendazole fungicide/parasiticide by SERS: quantitative analysis and adsorption mechanism. *Appl Surf Sci* 517:145786. <https://doi.org/10.1016/j.apsusc.2020.145786>
34. Zhang H, Cui Q, Xu L, Jiao A, Tian Y, Liu X, Li S, Li H, Chen M, Chen F (2020) Blue laser-induced photochemical synthesis of CuAg nanoalloys on h-BN supports with enhanced SERS activity for trace-detection of residual pesticides on tomatoes. *J Alloys Compd* 825:153996. <https://doi.org/10.1016/j.jallcom.2020.153996>
35. Liang P, Cao Y, Dong Q, Wang D, Jin S, Yu Z, Ye J, Zou M (2020) A balsam pear-shaped CuO SERS substrate with highly chemical enhancement for pesticide residue detection. *Microchim Acta* 187:335. <https://doi.org/10.1007/s00604-020-04303-w>
36. Barveen NR, Wang T-J, Chang Y-H (2020) Synergistic action of star-shaped Au/Ag nanoparticles decorated on AgFeO<sub>2</sub> for ultrasensitive SERS detection of a chemical warfare agent on real samples. *Anal Methods* 12(10):1342–1352. <https://doi.org/10.1039/C9AY02347J>